EUROPEAN ORGANIZATION FOR NUCLEAR RESEARCH (CERN)

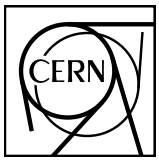

CERN-EP-2023-006
26 January 2023

Observation of new Ω_c^0 states decaying to the $\Xi_c^+ K^-$ final state

LHCb collaboration

Abstract

Two new excited states, $\Omega_c(3185)^0$ and $\Omega_c(3327)^0$, are observed in the $\Xi_c^+ K^-$ invariant-mass spectrum using proton-proton collision data collected by the LHCb experiment, corresponding to an integrated luminosity of $9\,\text{fb}^{-1}$. Five previously observed excited Ω_c^0 states are confirmed, namely $\Omega_c(3000)^0$, $\Omega_c(3050)^0$, $\Omega_c(3065)^0$, $\Omega_c(3090)^0$, and $\Omega_c(3119)^0$. The masses and widths of these seven states are measured with the highest precision to date.

Submitted to Phys. Rev. Lett.

Singly charmed baryons consist of one charm quark and two lighter quarks. Due to the large mass difference between the charm quark and the lighter quarks, the singly charmed baryon mass spectrum can be described systematically in heavy quark effective theory (HQET) [1]. Many excited states are expected by HQET because of the many degrees of freedom of the three-quark system. In 2017, the LHCb collaboration reported the observation of five new narrow Ω_c^0 states decaying to the $\Xi_c^+ K^-$ final state [2]. Four of them have been confirmed in e^+e^- collisions by the Belle collaboration [3] and in the $\Xi_c^+ K^-$ invariant-mass projection of $\Omega_b^- \to \Xi_c^+ K^- \pi^-$ decays by the LHCb collaboration [4]. The inclusion of charge-conjugate processes is implied throughout this Letter, unless stated otherwise.

Most theoretical studies interpret these states as excited bound states [5–21]; however, the schemes for matching their masses and quantum numbers are divergent among different studies. The lattice QCD calculation of Ref. [22] presents a rich invariant-mass spectrum, including dozens of D– or F–wave excited states. In other studies, the $\Omega_c(3050)^0$ and $\Omega_c(3090)^0$ states are interpreted as baryon-meson molecular (quasi-bound) states [23–25]. The most likely molecular structure of the $\Omega_c(3050)^0$ state is $\Xi_c^{\prime}\bar{K}$, and another possibility is $\Omega_c^0\eta$. The $\Omega_c(3090)^0$ state is argued to be a pure molecular state of ΞD. Finally, some theoretical studies [26, 27] also suggest the presence of three pentaquark states ($sscq\overline{q}$) with masses very close to the $\Omega_c(3065)^0$, $\Omega_c(3090)^0$, and $\Omega_c(3119)^0$ states, which may indicate the presence of a considerable $sscq\overline{q}$ component in these three Ω_c^0 baryons. In addition, another $sscq\overline{q}$ state is predicted with a mass of $\sim$2980 MeV (natural units are used throughout this Letter). The branching fractions of excited Ω_c^0 baryons to final states such as $\Xi_c\pi$, $\Omega_c\eta$, etc., may depend on the internal molecular or pentaquark structure of these baryons, and thus provide a way to elucidate their inner structure. Besides, searching for new excited states is another way to experimentally study the charmed baryon spectrum.

This Letter presents an updated analysis of the $\Xi_c^+ K^-$ invariant-mass spectrum, using proton-proton (pp) collision data collected by the LHCb experiment from 2011 to 2018 at center-of-mass energies of 7, 8 and 13 TeV, corresponding to integrated luminosities of 1, 2 and 6 fb^{-1}, respectively. Grouped by trigger strategy, data recorded in 2011–2015 is referred to as data set 1, and data collected in 2016–2018 is referred to as data set 2. The increased charm production cross section at higher center-of-mass energy, the higher integrated luminosity, and the improvement in the trigger system [28, 29] result in a five times larger sample size compared to the previous analysis [2]. The results presented in this Letter supersede the previous mass and width determinations [2].

The LHCb detector [30, 31] is a single-arm forward spectrometer covering the pseudorapidity range $2 < \eta < 5$, designed for the study of particles containing b or c quarks. Simulated data samples are produced with the software packages described in Refs. [32–36] and are used to develop the event selection, estimate the invariant-mass resolution, and model physics processes that may constitute peaking backgrounds in the analysis.

The $\Xi_c^+ (\to pK^-\pi^+)$ candidates are formed with three tracks that do not originate from any primary pp interaction vertex (PV) and have significant transverse momentum (p_{T}). Particle identification (PID) requirements are applied to all the final-state tracks in order to suppress combinatorial background. Additionally, PID vetoes are applied to suppress background from misidentified charm meson decays. These vetoes are formed by placing requirements on the invariant-mass of the candidates recomputed with the

relevant change in the particle mass hypothesis. The Ξ_c^+ candidates are required to have a large flight-distance significance from any PV and a small value of $\chi^2_{\rm IP}$, defined as the difference between the vertex fit χ^2 of the PV reconstructed with and without the particle in question. The reconstructed Ξ_c^+ candidates must have an invariant mass in the range of $[2450, 2485]$ MeV, corresponding to about three times the invariant-mass resolution around the known Ξ_c^+ mass [37]. Each Ξ_c^+ candidate is combined with a K^- candidate that originates from the same PV and has $p_{\rm T}$ greater than 0.4 GeV. The $\Xi_c^+K^-$ combinations with good vertex quality and $p_{\rm T}$ greater than 4.5 GeV are retained as $\Omega_c(X)^0$ candidates, where X is the mass of the excited state.

A multivariate classifier based on a boosted decision tree (BDT) algorithm [38] and implemented in the TMVA [39] toolkit is used to further improve the signal purity. The variables used to train the BDT classifier are: the χ^2 value of the Ξ_c^+ decay-vertex fit, the Ξ_c^+ flight distance, the angle between the Ξ_c^+ momentum vector and the line that connects the Ξ_c^+ decay vertex with its PV, the $\chi^2_{\rm IP}$ and $p_{\rm T}$ of Ξ_c^+ and $\Omega_c(X)^0$ candidates; and the $\chi^2_{\rm IP}$, $p_{\rm T}$ and particle-identification variables of all final state particles. Due to the difference in trigger strategies, different BDT classifiers are used for data sets 1 and 2. The BDT classifier is trained with simulated signal decays generated with the 2012 (2016) configuration for data set 1 (data set 2), and background candidates taken from the Ξ_c^+ invariant-mass sideband region, defined as $[2400, 2440]$ MeV and $[2500, 2540]$ MeV. The working points are chosen such that the BDT classifier efficiency on the signal is 75%; no fine-tuned optimization is performed to avoid favoring any particular excited state.

To improve the mass resolution, the variable $m(\Xi_c^+K^-)$ is defined as the difference between the invariant mass of the $\Omega_c(X)^0$ and Ξ_c^+ candidates, to which the known Ξ_c^+ mass [37] is added. The $\Xi_c^+K^-$ invariant-mass distribution is shown in Fig. 1, where seven peaking structures are seen. Five of them have been observed in the previous analysis [2], while the $\Omega_c(3185)^0$ and $\Omega_c(3327)^0$ states are observed for the first time. There are no similar structures in the wrong-sign sample ($\Xi_c^+K^+$) or in the spectrum of Ξ_c^+ sideband candidates combined with a kaon.

To determine the masses and widths of these $\Omega_c(X)^0$ states, an extended maximum likelihood fit with bin widths of 1 MeV is performed to the $\Xi_c^+K^-$ invariant-mass distributions, simultaneously to data sets 1 and 2. The $\Omega_c(X)^0$ contributions are described by S-wave relativistic Breit–Wigner functions convolved with a Gaussian resolution function whose width is determined from simulated signal samples. The combinatorial background is parameterized by an empirical function,

$$B(\Delta m) = (\Delta m)^a \times \exp(b_1\Delta m + b_2\Delta m^2), \tag{1}$$

where Δm is the difference between the invariant mass of the $\Xi_c^+K^-$ candidate and the $\Xi_c^+K^-$ mass threshold, and a, b_1 and b_2 are free parameters. In addition, three feed-down components from partially reconstructed decays of the $\Omega_c(3065)^0$, $\Omega_c(3090)^0$, and $\Omega_c(3119)^0$ resonances are included. These contributions are from $\Omega_c(X)^0 \to \Xi_c'^+(\to \Xi_c^+\gamma)K^-$ decays, where the photon is not reconstructed. Their shapes are determined from simulated samples and are fixed, while their yields are free to vary in the fit.

The fit results are shown in Fig. 1 and summarized in Table 1. In addition to the five narrow states at lower invariant mass that were previously observed, two new states with masses of about 3185 MeV and 3327 MeV, denoted $\Omega_c(3185)^0$ and $\Omega_c(3327)^0$ are observed with high significance.

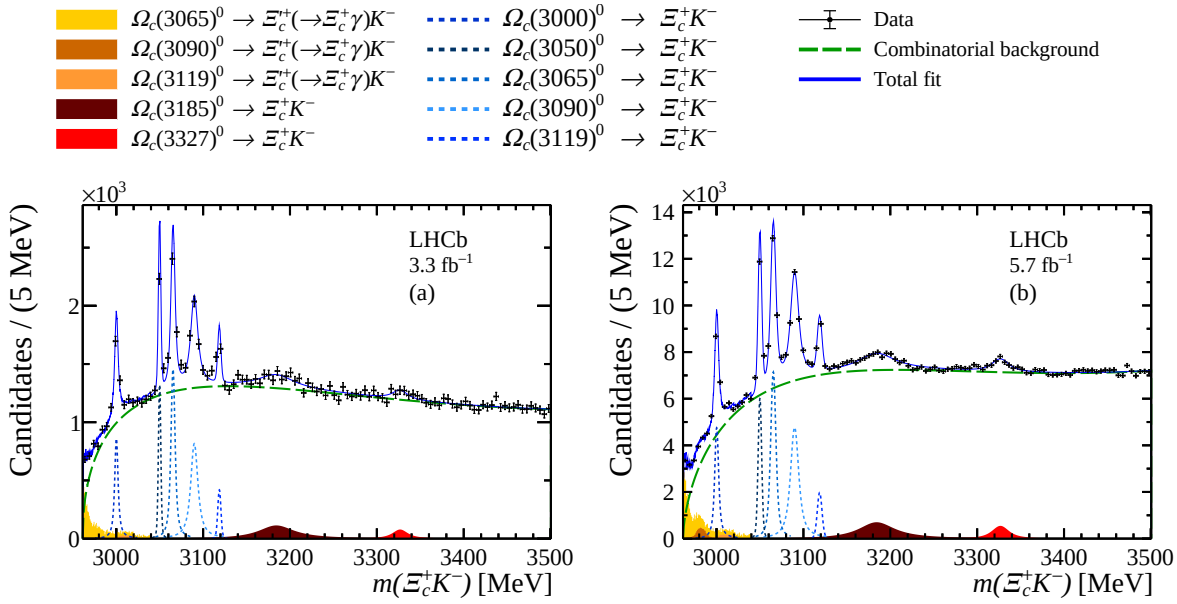

Figure 1: Invariant-mass distribution of the $\Omega_c(X)^0$ candidates in (a) data set 1 and (b) data set 2, with the fit results overlaid. A bin width of 5 MeV is used for plotting. The previously observed excited Ω_c^0 states are shown in blue dashed lines. The $\Omega_c(3185)^0$ state is shown in the brown area, and the $\Omega_c(3327)^0$ state is shown in the red area. Three feed-down components are shown as the yellow areas, while the green long-dashed line corresponds to the combinatorial background.

The enhancement around the $\Xi_c^+K^-$ mass threshold is described by the partially reconstructed decays of $\Omega_c(X)^0 \to \Xi_c'^+(\to \Xi_c^+\gamma)K^-$, as was done in the previous analysis [2]. In the exclusive analysis using the $\Omega_b^- \to \Omega_c(X)^0(\to \Xi_c^+K^-)\pi^-$ decay [4], these feed-down components are excluded by requiring an appropriate signal mass window of the Ω_b^- baryon, while the threshold enhancement is still present. In the Ω_b^- analysis this structure was modeled as an S-wave Breit–Wigner distribution, but the available data in Ref. [4] are not sufficient to determine this structure. To check if this structure

Table 1: Fit results of the mass, width, and yield for each state, and for each data set. Uncertainties are statistical only.

Resonance	m (MeV)	Γ (MeV)	Yield (data set 1)	Yield (data set 2)
$\Omega_c(3000)^0$	3000.44 ± 0.07	3.83 ± 0.23	1225 ± 83	7533 ± 263
$\Omega_c(3050)^0$	3050.18 ± 0.04	0.67 ± 0.17	1139 ± 65	7379 ± 215
$\Omega_c(3065)^0$	3065.63 ± 0.06	3.79 ± 0.20	2180 ± 99	13046 ± 316
$\Omega_c(3090)^0$	3090.16 ± 0.11	8.48 ± 0.44	2234 ± 136	14434 ± 486
$\Omega_c(3119)^0$	3118.98 ± 0.12	0.60 ± 0.63	470 ± 66	3279 ± 234
$\Omega_c(3185)^0$	3185.1 ± 1.7	50 ± 7	1642 ± 367	10278 ± 1565
$\Omega_c(3327)^0$	3327.1 ± 1.2	20 ± 5	489 ± 173	3649 ± 723

is present in this analysis, the enhancement is fitted using two alternative models: a Breit–Wigner component with and without the feed down coming from the $\Omega_c(3065)^0$ contribution. The yield of the $\Omega_c(3065)^0$ feed down is constrained to be 10% of the $\Omega_c(3065)^0$ signal yield for the former. This constraint is equivalent to fixing the ratio $\mathcal{B}(\Omega_c(3065)^0 \to \Xi_c'^+ K^-) \times \mathcal{B}(\Xi_c'^+ \to \Xi_c^+\gamma)/\mathcal{B}(\Omega_c(3065)^0 \to \Xi_c^+ K^-)$ to 0.1, which is chosen due to the small phase space of the $\Omega_c(3065)^0 \to \Xi_c'^+ K^-$ decay. The yields of the other feed-down contributions are free to float. Unfortunately, the shape of the $\Omega_c(3065)^0$ feed down and the additional Breit–Wigner structure are too similar to be separated in this analysis. The relative contributions from these two components can not be determined from data, and hence this is accounted for as a systematic uncertainty. The existence of another hidden state cannot be excluded.

The mass difference between the $\Omega_c(3185)^0$ and $\Omega_c(3327)^0$ baryons is approximately the mass of the pion. It is possible that partially reconstructed candidates from the $\Omega_c(3327)^0$ decay fall into the $\Omega_c(3185)^0$ region, such as $\Omega_c(3327)^0 \to \Xi_c(2645)^+(\to \Xi_c^+\pi^0)K^-$ and $\Omega_c(3327)^0 \to \Xi_c'^+(\to \Xi_c^+\gamma)K^-$ decays with the π^0 or γ not reconstructed. The $m(\Xi_c^+ K^-)$ line shapes of such contributions are obtained using the fast simulation toolkit RapidSim [40]. The feed-down contributions have been studied under different spin structure hypotheses, and differences from phase-space simulation were found to be negligible. The fit favors the presence of the $\Omega_c(3327)^0$ feed down with the π^0 missing. The $\Omega_c(3327)^0$ feed down strongly affects the measured mass and width of the $\Omega_c(3185)^0$ baryon, and is assigned as a systematic uncertainty. None of the models for the $\Omega_c(3185)^0$ region can be ruled out. In addition, the effects of the three-body decay $\Omega_c(3327)^0 \to \Xi_c^+ K^-\pi^0$ are checked with a uniform phase-space model, and found to be insignificant on any of the states when assuming the ratio $\mathcal{B}(\Omega_c(3327)^0 \to \Xi_c^+ K^-\pi^0)/\mathcal{B}(\Omega_c(3327)^0 \to \Xi_c^+ K^-)$ to be unity.

The effects of the $\Xi_c(3055)^0 \to \Xi_c'^+(\to \Xi_c^+\gamma)\pi^-$, $\Xi_c(3055)^0 \to \Xi_c(2645)^+(\to \Xi_c^+\pi^0)\pi^-$, and $\Xi_c(2923/2939/2965)^0 \to \Xi_c^+\pi^-$ decays, for which the pion is misidentified as a kaon and the π^0/γ from the $\Xi_c(2645)^+/\Xi_c'^+$ decays is missing, are studied and found to be negligible. The contribution from $\Omega_c(3327)^0 \to \Xi_c^+ K^{*-}$ is kinematically suppressed.

Several checks are performed to confirm the existence of the observed states and the stability of the fitted parameters. Each data set is divided into subsamples according to data-taking conditions, charge combination ($\Xi_c^+ K^-$ or $\Xi_c^- K^+$), or different intervals of $p_{\rm T}(K^-)$ and $p_{\rm T}(\Xi_c^+)$. In all tests, the results are consistent with the default fit. A two-peak structure also describes the data well in the mass region around 3185 MeV, hence the presence of two states in this region can not be excluded. The bias from the fit model itself is estimated using pseudoexperiments. For each parameter, the mean differences between the fitted values and the input ones are included as systematic uncertainties.

The uncertainty related to the signal model is estimated by fitting the data with variations in the spin hypotheses and the Blatt-Weisskopf factor [41]. The systematic uncertainty from the combinatorial background model is estimated by using a fourth-order Chebyshev polynomial as an alternative function. In addition, a systematic uncertainty is assigned based on the spread of results obtained by performing the fit with different bin widths.

Some sources of systematic uncertainty only contribute to the mass measurement, including the momentum calibration for charged particles, which has a relative accuracy of 0.03% [42, 43], and the energy loss due to the imperfect modeling of the detector material, which results in a 0.04 MeV uncertainty. The differences between simulation and data

Table 2: Systematic uncertainties on the measured masses and natural widths.

Source [MeV, MeV]	$\Omega_c(3000)^0$ $[m,\ \Gamma]$	$\Omega_c(3050)^0$ $[m,\ \Gamma]$	$\Omega_c(3065)^0$ $[m,\ \Gamma]$	$\Omega_c(3090)^0$ $[m,\ \Gamma]$	$\Omega_c(3119)^0$ $[m,\ \Gamma]$	$\Omega_c(3185)^0$ $[m,\ \Gamma]$	$\Omega_c(3327)^0$ $[m,\ \Gamma]$
Threshold structure	$[^{+0.01}_{-0.07},\ ^{+1.23}_{-0.19}]$	$[^{+0.00}_{-0.01},\ ^{+0.00}_{-0.17}]$	$[^{+0.01}_{-0.00},\ ^{+0.00}_{-0.11}]$	$[^{+0.01}_{-0.00},\ ^{+0.12}_{-0.20}]$	$[^{+0.06}_{-0.00},\ ^{+0.00}_{-0.16}]$	$[^{+0.32}_{-0.57},\ ^{+8.05}_{-0.83}]$	$[^{+0.01}_{-0.15},\ ^{+1.71}_{-0.04}]$
feed down from $\Omega_c^0(3327)$	$[^{+0.04}_{-0.00},\ ^{+0.04}_{-0.00}]$	$[^{+0.00}_{-0.00},\ ^{+0.00}_{-0.01}]$	$[^{+0.01}_{-0.00},\ ^{+0.03}_{-0.00}]$	$[^{+0.01}_{-0.00},\ ^{+0.22}_{-0.00}]$	$[^{+0.01}_{-0.00},\ ^{+0.07}_{-0.00}]$	$[^{+4.28}_{-0.00},\ ^{+0.00}_{-10.81}]$	$[^{+0.00}_{-0.20},\ ^{+0.98}_{-0.00}]$
Fit bias	$[^{+0.02}_{-0.00},\ ^{+0.01}_{-0.00}]$	$[^{+0.02}_{-0.00},\ ^{+0.12}_{-0.00}]$	$[^{+0.00}_{-0.00},\ ^{+0.08}_{-0.00}]$	$[^{+0.01}_{-0.00},\ ^{+0.20}_{-0.00}]$	$[^{+0.00}_{-0.02},\ ^{+0.40}_{-0.00}]$	$[^{+0.00}_{-0.37},\ ^{+4.84}_{-0.00}]$	$[^{+0.00}_{-0.18},\ ^{+0.00}_{-0.70}]$
Spin and radius	$[^{+0.01}_{-0.01},\ ^{+0.01}_{-0.01}]$	$[^{+0.01}_{-0.01},\ ^{+0.01}_{-0.01}]$	$[^{+0.01}_{-0.01},\ ^{+0.02}_{-0.01}]$	$[^{+0.01}_{-0.01},\ ^{+0.05}_{-0.01}]$	$[^{+0.01}_{-0.01},\ ^{+0.06}_{-0.01}]$	$[^{+0.01}_{-0.18},\ ^{+0.56}_{-0.01}]$	$[^{+0.01}_{-0.02},\ ^{+0.01}_{-0.60}]$
Background	$[^{+0.04}_{-0.00},\ ^{+0.98}_{-0.00}]$	$[^{+0.00}_{-0.01},\ ^{+0.00}_{-0.18}]$	$[^{+0.00}_{-0.00},\ ^{+0.00}_{-0.29}]$	$[^{+0.00}_{-0.06},\ ^{+0.00}_{-1.58}]$	$[^{+0.00}_{-0.21},\ ^{+0.00}_{-0.60}]$	$[^{+5.98}_{-0.00},\ ^{+0.00}_{-16.2}]$	$[^{+0.00}_{-1.24},\ ^{+12.9}_{-0.00}]$
Bin size	$[^{+0.00}_{-0.10},\ ^{+0.06}_{-0.04}]$	$[^{+0.00}_{-0.01},\ ^{+0.40}_{-0.03}]$	$[^{+0.02}_{-0.03},\ ^{+0.08}_{-0.07}]$	$[^{+0.01}_{-0.05},\ ^{+0.37}_{-0.09}]$	$[^{+0.00}_{-0.06},\ ^{+0.00}_{-0.60}]$	$[^{+0.14}_{-0.48},\ ^{+2.75}_{-0.50}]$	$[^{+0.07}_{-0.00},\ ^{+1.16}_{-0.00}]$
Momentum calibration	$[\pm 0.01,\ -\ ]$	$[\pm 0.03,\ -\ ]$	$[\pm 0.03,\ -\ ]$	$[\pm 0.04,\ -\ ]$	$[\pm 0.05,\ -\ ]$	$[\pm 0.07,\ -\ ]$	$[\pm 0.11,\ -\ ]$
Energy loss	$[\pm 0.04,\ -\ ]$	$[\pm 0.04,\ -\ ]$	$[\pm 0.04,\ -\ ]$	$[\pm 0.04,\ -\ ]$	$[\pm 0.04,\ -\ ]$	$[\pm 0.04,\ -\ ]$	$[\pm 0.04,\ -\ ]$
Simulation/Data difference	$[^{+0.00}_{-0.01},\ ^{+0.20}_{-0.22}]$	$[^{+0.01}_{-0.04},\ ^{+0.48}_{-0.67}]$	$[^{+0.01}_{-0.00},\ ^{+0.36}_{-0.35}]$	$[^{+0.00}_{-0.02},\ ^{+0.36}_{-0.29}]$	$[^{+0.03}_{-0.00},\ ^{+0.80}_{-0.59}]$	$[^{+0.08}_{-0.34},\ ^{+2.58}_{-0.67}]$	$[^{+0.02}_{-0.05},\ ^{+0.27}_{-0.28}]$
Total	$[^{+0.07}_{-0.13},\ ^{+1.59}_{-0.29}]$	$[^{+0.06}_{-0.07},\ ^{+0.64}_{-0.72}]$	$[^{+0.06}_{-0.06},\ ^{+0.38}_{-0.47}]$	$[^{+0.06}_{-0.10},\ ^{+0.61}_{-1.62}]$	$[^{+0.09}_{-0.23},\ ^{+0.90}_{-1.05}]$	$[^{+7.36}_{-0.92},\ ^{+10.1}_{-19.5}]$	$[^{+0.14}_{-1.28},\ ^{+13.1}_{-0.96}]$

Table 3: Measured mass and natural width for each of the seven $\Omega_c(X)^0$ states. The first uncertainty is statistical and the second is systematic, the third (mass only) arises from the uncertainty of the known Ξ_c^+ mass.

Resonance	m (MeV)	Γ (MeV)
$\Omega_c(3000)^0$	$3000.44 \pm 0.07\ ^{+0.07}_{-0.13} \pm 0.23$	$3.83 \pm 0.23\ ^{+1.59}_{-0.29}$
$\Omega_c(3050)^0$	$3050.18 \pm 0.04\ ^{+0.06}_{-0.07} \pm 0.23$	$0.67 \pm 0.17\ ^{+0.64}_{-0.72}$
		$< 1.8\,\text{MeV}, 95\%$ C.L.
$\Omega_c(3065)^0$	$3065.63 \pm 0.06\ ^{+0.06}_{-0.06} \pm 0.23$	$3.79 \pm 0.20\ ^{+0.38}_{-0.47}$
$\Omega_c(3090)^0$	$3090.16 \pm 0.11\ ^{+0.06}_{-0.10} \pm 0.23$	$8.48 \pm 0.44\ ^{+0.61}_{-1.62}$
$\Omega_c(3119)^0$	$3118.98 \pm 0.12\ ^{+0.09}_{-0.23} \pm 0.23$	$0.60 \pm 0.63\ ^{+0.90}_{-1.05}$
		$< 2.5\,\text{MeV}, 95\%$ C.L.
$\Omega_c(3185)^0$	$3185.1 \pm 1.7\ ^{+7.4}_{-0.9} \pm 0.2$	$50 \pm 7\ ^{+10}_{-20}$
$\Omega_c(3327)^0$	$3327.1 \pm 1.2\ ^{+0.1}_{-1.3} \pm 0.2$	$20 \pm 5\ ^{+13}_{-1}$

mainly affect the measurement of the natural width of each state. It is calculated by varying the width of the resolution function by 10% [44].

The systematic uncertainties are summarized in Table 2. After considering the systematic uncertainty, the significances of the $\Omega_c(3185)^0$ and $\Omega_c(3327)^0$ states are larger than $12\,\sigma$ and $10\,\sigma$, respectively. The significance for each state is determined from Wilk's theorem using the difference in log-likelihood with and without that signal component. Other assumptions, such as the two-peak structure, additional feed-down components or a combination of them cannot be excluded, and are included in the systematic uncertainties. The results of the measured mass and natural width of all seven states , shown in Table 3, are the most precise to date, and supersede those in Ref. [2]. The correlations between these results and those in Ref. [4] are negligible, except for the systematic uncertainty due to the momentum calibration and energy loss, which are fully correlated. The natural widths of the $\Omega_c(3050)^0$ and $\Omega_c(3119)^0$ baryons are very close to zero; therefore upper limits on them are set at Bayesian 95% confidence level, assuming Gaussian behavior for both statistical and systematic uncertainties.

In conclusion, the $\Xi_c^+ K^-$ invariant-mass spectrum is investigated using pp collision data corresponding to a total integrated luminosity of $9\,\text{fb}^{-1}$ collected by the LHCb experiment. A high-purity sample of Ξ_c^+ candidates is selected using the Cabibbo-suppressed decay $\Xi_c^+ \to pK^+\pi^-$. A total of seven excited states is observed: $\Omega_c(3000)^0$, $\Omega_c(3050)^0$, $\Omega_c(3065)^0$, $\Omega_c(3090)^0$, $\Omega_c(3119)^0$, $\Omega_c(3185)^0$, and $\Omega_c(3327)^0$, of which the $\Omega_c(3185)^0$ and $\Omega_c(3327)^0$ states are observed for the first time, with masses near the threshold of the ΞD and ΞD^* final states. Referring to the lattice QCD result of Ref. [22], the $\Omega_c(3185)^0$ mass is in the predicted range for P-wave states, and the $\Omega_c(3327)^0$ mass is in the range for many possible states. The quantum numbers of these states remain to be determined.

References

[1] A. G. Grozin, *Introduction to the heavy quark effective theory. part 1*, arXiv:hep-ph/9908366.

[2] LHCb collaboration, R. Aaij *et al.*, *Observation of five new narrow Ω_c^0 states decaying to $\Xi_c^+ K^-$*, Phys. Rev. Lett. **118** (2017) 182001, arXiv:1703.04639.

[3] Belle collaboration, J. Yelton *et al.*, *Observation of excited Ω_c charmed baryons in e^+e^- collisions*, Phys. Rev. **D97** (2018) 051102, arXiv:1711.07927.

[4] LHCb collaboration, R. Aaij *et al.*, *Observation of excited Ω_c^0 baryons in $\Omega_b^- \to \Xi_c^+ K^- \pi^+$ decays*, Phys. Rev. **D104** (2021) L091102, arXiv:2107.03419.

[5] M. Karliner and J. L. Rosner, *Very narrow excited Ω_c baryons*, Phys. Rev. **D95** (2017) 114012, arXiv:1703.07774.

[6] H.-X. Chen *et al.*, *Decay properties of P-wave charmed baryons from light-cone QCD sum rules*, Phys. Rev. **D95** (2017) 094008, arXiv:1703.07703.

[7] K.-L. Wang, L.-Y. Xiao, X.-H. Zhong, and Q. Zhao, *Understanding the newly observed Ω_c states through their decays*, Phys. Rev. **D95** (2017) 116010, arXiv:1703.09130.

[8] W. Wang and R.-L. Zhu, *Interpretation of the newly observed Ω_c^0 resonances*, Phys. Rev. **D96** (2017) 014024, arXiv:1704.00179.

[9] H.-Y. Cheng and C.-W. Chiang, *Quantum numbers of Ω_c states and other charmed baryons*, Phys. Rev. **D95** (2017) 094018, arXiv:1704.00396.

[10] Z. Zhao, D.-D. Ye, and A. Zhang, *Hadronic decay properties of newly observed Ω_c baryons*, Phys. Rev. **D95** (2017) 114024, arXiv:1704.02688.

[11] S. S. Agaev, K. Azizi, and H. Sundu, *Interpretation of the new Ω_c^0 states via their mass and width*, Eur. Phys. J. **C77** (2017) 395, arXiv:1704.04928.

[12] B. Chen and X. Liu, *New Ω_c^0 baryons discovered by LHCb as the members of $1P$ and $2S$ states*, Phys. Rev. **D96** (2017) 094015, arXiv:1704.02583.

[13] Z.-G. Wang, *Analysis of $\Omega_c(3000)$, $\Omega_c(3050)$, $\Omega_c(3066)$, $\Omega_c(3090)$ and $\Omega_c(3119)$ with QCD sum rules*, Eur. Phys. J. **C77** (2017) 325, arXiv:1704.01854.

[14] K.-L. Wang, Y.-X. Yao, X.-H. Zhong, and Q. Zhao, *Strong and radiative decays of the low-lying S- and P-wave singly heavy baryons*, Phys. Rev. **D96** (2017) 116016, arXiv:1709.04268.

[15] Y.-X. Yao, K.-L. Wang, and X.-H. Zhong, *Strong and radiative decays of the low-lying D-wave singly heavy baryons*, Phys. Rev. **D98** (2018) 076015, arXiv:1803.00364.

[16] Q. Mao *et al.*, *D-wave heavy baryons of the $SU(3)$ flavor $\mathbf{6}_F$*, Phys. Rev. **D96** (2017) 074021, arXiv:1707.03712.

[17] E. Santopinto *et al.*, *The Ω_c-puzzle solved by means of quark model predictions*, Eur. Phys. J. **C79** (2019) 1012, arXiv:1811.01799.

[18] H.-g. Xu *et al.*, *Study on the Ω_c^0 states decaying to $\Xi_c^+ K^-$ in pp collisions at $\sqrt{s} = 7$, 13 TeV*, Phys. Rev. **C102** (2020) 054319, arXiv:1912.12905.

[19] S. Hu, G. Meng, and F. Xu, *Hadronic weak decays of the charmed baryon Ω_c*, Phys. Rev. **D101** (2020) 094033, arXiv:2003.04705.

[20] H.-M. Yang and H.-X. Chen, *P-wave charmed baryons of the SU(3) flavor 6F*, Phys. Rev. **D104** (2021) 034037, arXiv:2106.15488.

[21] A. Ramirez Morales, *Strong decay widths and mass spectra of charmed baryons*, PoS **ICHEP2022** (2022) 913.

[22] M. Padmanath and N. Mathur, *Quantum numbers of recently discovered Ω_c^0 baryons from lattice QCD*, Phys. Rev. Lett. **119** (2017) 042001, arXiv:1704.00259.

[23] V. R. Debastiani, J. M. Dias, W. H. Liang, and E. Oset, *Molecular Ω_c states generated from coupled meson-baryon channels*, Phys. Rev. **D97** (2018) 094035, arXiv:1710.04231.

[24] G. Montaña, A. Feijoo, and A. Ramos, *A meson-baryon molecular interpretation for some Ω_c excited states*, Eur. Phys. J. **A54** (2018) 64, arXiv:1709.08737.

[25] A. Ramos, A. Feijoo, Q. Llorens, and G. Montaña, *The molecular nature of some exotic hadrons*, Few Body Syst. **61** (2020) 34, arXiv:2009.04367.

[26] C. S. An and H. Chen, *Observed Ω_c^0 resonances as pentaquark states*, Phys. Rev. **D96** (2017) 034012, arXiv:1705.08571.

[27] H.-J. Wang, Z.-Y. Di, and Z.-G. Wang, *Analysis of the excited Ω_c states as the $\frac{1}{2}^{\pm}$ pentaquark states with QCD sum rules*, Communications in Theoretical Physics **73** (2021) 035201.

[28] R. Aaij *et al.*, *The LHCb trigger and its performance in 2011*, JINST **8** (2013) P04022, arXiv:1211.3055.

[29] R. Aaij *et al.*, *Design and performance of the LHCb trigger and full real-time reconstruction in Run 2 of the LHC*, JINST **14** (2019) P04013, arXiv:1812.10790.

[30] LHCb collaboration, A. A. Alves Jr. *et al.*, *The LHCb detector at the LHC*, JINST **3** (2008) S08005.

[31] LHCb collaboration, R. Aaij *et al.*, *LHCb detector performance*, Int. J. Mod. Phys. **A30** (2015) 1530022, arXiv:1412.6352.

[32] T. Sjöstrand, S. Mrenna, and P. Skands, *A brief introduction to PYTHIA 8.1*, Comput. Phys. Commun. **178** (2008) 852, arXiv:0710.3820.

[33] LHCb collaboration, I. Belyaev *et al.*, *Handling of the generation of primary events in Gauss, the LHCb simulation framework*, J. Phys. Conf. Ser. **331** (2011) 032047.

[34] D. J. Lange, *The EvtGen particle decay simulation package*, Nucl. Instrum. Meth. **A462** (2001) 152.

[35] Geant4 collaboration, J. Allison *et al.*, *Geant4 developments and applications*, IEEE Trans. Nucl. Sci. **53** (2006) 270.

[36] LHCb collaboration, M. Clemencic *et al.*, *The LHCb simulation application, Gauss: Design, evolution and experience*, J. Phys. Conf. Ser. **331** (2011) 032023.

[37] Particle Data Group, R. L. Workman and Others, *Review of particle physics*, PTEP **2022** (2022) 083C01.

[38] V. V. Gligorov and M. Williams, *Efficient, reliable and fast high-level triggering using a bonsai boosted decision tree*, JINST **8** (2013) P02013, arXiv:1210.6861.

[39] A. Hoecker *et al.*, *TMVA 4 — toolkit for multivariate data analysis with ROOT, users guide*, arXiv:physics/0703039.

[40] G. A. Cowan, D. C. Craik, and M. D. Needham, *RapidSim: an application for the fast simulation of heavy-quark hadron decays*, Comput. Phys. Commun. **214** (2017) 239, arXiv:1612.07489.

[41] J. M. Blatt and V. F. Weisskopf, *Theoretical nuclear physics*, Springer, New York, 1952.

[42] LHCb collaboration, R. Aaij *et al.*, *Measurements of the Λ_b^0, Ξ_b^-, and Ω_b^- baryon masses*, Phys. Rev. Lett. **110** (2013) 182001, arXiv:1302.1072.

[43] LHCb collaboration, R. Aaij *et al.*, *Precision measurement of D meson mass differences*, JHEP **06** (2013) 065, arXiv:1304.6865.

[44] LHCb collaboration, R. Aaij *et al.*, *Precision measurement of the mass and lifetime of the Ξ_b^- baryon*, Phys. Rev. Lett. **113** (2014) 242002, arXiv:1409.8568.